Dynamical Treatment of Charge Transfer through Duplex Nucleic Acids Containing Modified Adenines

Giorgia Brancolini,[†,*] Agostino Migliore,[‡,§] Stefano Corni,[†] Miguel Fuentes-Cabrera,[⊥] F. Javier Luque,[∥] and Rosa Di Felice[†,#,*]

[†]CNR Institute of Nanoscience, S3 Center, Via Campi 213/A, 41125 Modena, Italy, [‡]School of Chemistry, Tel Aviv University, 69978 Tel Aviv, Israel, [§]Department of Chemistry, Duke University, Durham, North Carolina 27708, United States, [⊥]Center for Nanophase Materials Sciences, and Computer Science and Mathematics Division, Oak Ridge National Laboratory, P.O. Box 2008, Oak Ridge, Tennessee 37831-6494, United States, [∥]Department de Fisicoquímica and Institut de Biomedicina (IBUB), Facultat de Farmàcia, Universitat de Barcelona, Avenida Diagonal 643, Barcelona 08028, Spain, and [#]Department of Physics and Astronomy, University of Southern California, Los Angeles, California 90089 United States

ABSTRACT We address the issue of whether chemical alterations of nucleobases are an effective tool to modulate charge transfer through DNA molecules. Our investigation uses a multilevel computational approach based on classical molecular dynamics and quantum chemistry. We find yet another piece of evidence that structural fluctuations are a key factor to determine the electronic structure of double-stranded DNA. We argue that the electronic structure and charge transfer ability of flexible polymers is the result of a complex intertwining of various structural, dynamical and chemical factors. Chemical intuition may be used to design molecular wires, but this is not the sole component in the complex charge transfer mechanism through DNA.

KEYWORDS: DNA · chemical alterations · electronic structure · molecular dynamics · charge transfer

The issue of charge transfer in DNA has been generally addressed in the context of DNA damage and repair due to its implications in cancer development and therapeutics. A renewed interest in the electronic structure of DNA-based polymers has been recently stimulated by the quest for the development of molecular electronics.[1,2] The use of DNA as template for the design of nanowires is supported by the structural stability of the DNA duplex, the specific self-assembly properties between complementary bases, the possibility of incorporating a wide range of chemically modified constituents, and the availability of biotechnological tools that enable their large-scale synthesis.

One of the main challenges in the usage of DNA-based nanodevices in molecular circuits is the control of their electrical conductivity. Early work in this field has yielded seemingly controversial results for native DNA,[2] showing electrical behaviors from insulating through semiconducting to conducting, with even a report of proximity-induced superconductivity. However, a survey of the literature[2] highlighted that the variety of available experiments cannot be analyzed in a unique way. For instance, electrical measurements conducted on single molecules, bundles and networks, are not able to reveal a uniform interpretation scheme for the conductivity of DNA, because they refer to different materials. In addition, the experimental conditions were often variable. The current status may thus be schematically summarized as follows: (i) charges may be transported with relatively poor conductivity in short single DNA molecules or in longer molecules organized in bundles and networks; (ii) charge flow is blocked for long molecules deposited onto "hard" inorganic substrates. A plausible explanation was that the inability to conduct might arise from strong deformations induced by the substrate,[2,3] which is supported by recent experiments performed using suspended molecules.[4−6]

* Address correspondence to giorgia.brancolini@nano.cnr.it, rosa.difelice@unimore.it.

Received for review August 9, 2013 and accepted September 23, 2013.

Published online September 23, 2013
10.1021/nn404165y

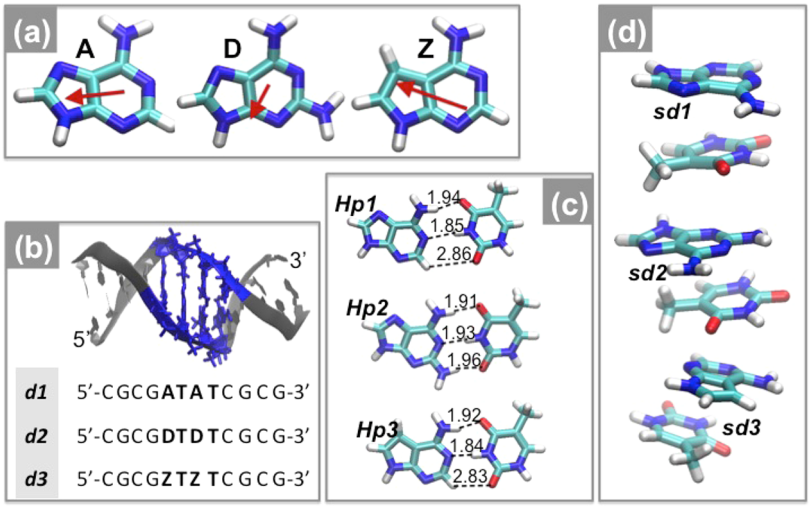

Figure 1. (a) Three-dimensional (3D) structure of adenine (A), diaminopurine (D) and deazaadenine (Z). The red arrow indicates the dipole moment of the molecule, which is 2.56, 1.33, and 3.34 D for A, D and Z, respectively (determined at the BHH/cc-pVTZ level of theory). (b) 3D structure of the most representative duplex dodecamer *d2* that contains D in the center of the sequence. The simulated sequences are indicated below the image. The acronyms *d1*, *d2* and *d3* are used for the three different duplex structures. (c) Hydrogen-bonded base pairs *Hp1* (A−T), *Hp2* (D−T) and *Hp3* (Z−T) used as test systems in force field parametrization, with indication of the H-bond lengths. (d) Stacked dimers *sd1* (A:T), *sd2* (D:T) and *sd3* (Z:T) used as test systems in force field parametrization.

In this context, the research in DNA-based electronics has followed two main strategies, which pursue either to minimize substrate-induced deformations (*i.e.*, suspended-molecule measurements,[4−7] or use of a soft organic buffer), or to exploit DNA-based molecular candidates with better intrinsic conductivity than natural DNA. This work explores the latter route by considering two specific DNA modifications that target the adenine (A) base by replacing it with deazaadenine (Z) and diaminopurine (D).

It is known that adenine−thymine (A−T) base pairs (bp) slow down the efficiency of charge transfer with respect to guanine−cytosine (G−C) tracts in DNA duplexes.[5,8] To solve this problem, Majima and coworkers[9,10] have recently investigated the effect of replacing A in A-tracts with Z and D. In Z the N_7 atom of A is replaced by a C−H group (Figure 1), which thus does not disturb the complementary base pairing with T. On the other hand, in D an amino group is attached to the C_2 hydrogen atom of the purine ring (Figure 1), which should thus enable the formation of an additional hydrogen bond with the carbonyl group at position 2 of T. The choice of D and Z was motivated by their lower ionization potential relative to A, and the experimental measurements revealed a sizable increase in the conductivity of the modified duplexes.[11,12]

Inspired by those experiments, the aim of this work is to investigate the effects triggered by the incorporation of either Z or D bases on the structural, electronic and charge transfer properties of DNA duplexes. To this end, a multilevel computational approach that combines classical molecular dynamics (MD) simulations and density functional theory (DFT) calculations of the ground-state electronic structure and transfer integrals has been adopted. The major aim is to explore the structural and electronic properties of the modified dimers relative to the canonical A−T base pair and to examine whether the low ionization potential of Z and D impacts the conductivity of DNA-based nanodevices. Previous theoretical efforts to understand charge transfer through modified DNA base pairs, including pairs with Z, were published already over a decade ago,[13,14] yet with no account of structural effects. One important development in recent studies on axial charge transfer through DNA is that the effects of dynamical disorder coming from internal nucleobase dynamics and mediated by the solvent environment play a critical role and cannot be treated as a small perturbation.[15−18] Our study includes such effects, as we explain below, and goes toward the simulation of realistic experimental conditions relevant for nanoscale applications. Overall, the investigation of charge transfer through natural and modified DNAs remains a hot research topic.[19]

RESULTS AND DISCUSSION

H-Bonding and Stacking Interactions for D and Z. Table 1 reports the results on the H-bonding and stacking interaction energies obtained at different levels of theory, as specified in the Materials and Methods. As expected, the presence of the additional amino group in D reinforces the H-bonded interaction energy in the D−T pair by *ca.* 3.5 kcal/mol compared to the A−T one. Likewise, replacement of A by Z leads to a lower stabilization of the H-bonded dimer (by 1.5 kcal/mol), which can be attributed to the enhanced dipole moment of Z relative to A (3.34 and 2.56 D, respectively). On the other hand, replacement of A by either D or Z leads to an enhancement of the stacking energies (by 0.6−1.0 kcal/mol).

TABLE 1. Interaction Energies (kcal/mol) for the H-Bonded Pairs and Stacked Dimers Illustrated in Figure 1c,d Obtained from Classical (AMBER) and Quantum (DFT, MP2, M062X) Calculations

		ΔE_{AMBER}	ΔE_{DFT}[a]	ΔE_{MP2}[b]
H-bonded pairs	A—T	−15.8	−13.1	−14.3
	D—T	−18.8	−16.6	−17.5
	Z—T	−17.5	−14.6	−14.7
stacked dimers	A:T	−6.9	−5.6	−5.4
	D:T	−7.4	−6.6	−6.0
	Z:T	−7.4	−6.6	−6.0

[a] Energies determined from BHH/cc-pVTZ and M062X/6-31+G(d) levels for H-bonded and stacked pairs, respectively. [b] Energies of H-bonded pairs and stacked dimers are obtained from MP2/6-31G(d) and MP2/6-31G(d,0.25) calculations, respectively. The need for different exponents of d-polarization functions was explained elsewhere.[24]

Classical calculations reproduce correctly the trends observed from quantum chemical (QM) interaction energies, though AMBER results show a slight overestimation of the MP2 and DFT values. The relative discrepancies between the MM and QM data are modestly enlarged in the case of stacking interactions. Despite the obvious simplicity of the force field, the agreement achieved reinforces the confidence in the quality of the AMBER parameters to represent interactions involving D and Z bases in solution. This conclusion is supported by the comparison with previously developed parameters for DNA nucleotides at the same level of theory.[20−23] The positive benchmark of MM results against different levels of QM results is a good index of reliable portability.

Molecular Dynamics Trajectories. The MD trajectories support the structural integrity of the duplexes, as noted in root-mean-square deviations of about 2.0−2.5 Å relative to the respective equilibrated structure (see Figure S1 in Supporting Information). Inspection of the average structures (derived from the snapshots collected along 20 ns) reveals a close structural similarity between the three duplexes, suggesting the lack of significant structural alterations that might rise from the replacement of A by either D or Z. In fact, the RMSD between the heavy atoms of the central quintuplet GXTXT (X: A, D or Z) varies from 0.37 to 0.48 Å between the three average structures, and the backbone RMSD over the entire oligomers between the three average structures is 1.2−1.4 Å.

Besides the similarity in the overall structural features of the duplexes, the analysis of the helical parameters also supports the integrity of the duplexes. In general the average values of the helical parameters do not exhibit significant differences. As an example, the results obtained for the rise and twist values of the central triplet GXT triplet (X: A, D or Z) are summarized in Table 2, which reports the weighted average (weights in Table S2, Supporting Information) over the 10 representative structures for each of the oligomers *d1*, *d2* and *d3*

TABLE 2. Inter-bp Parameters Rise and Twist in the Central Trimers 5′-GAT-3′, 5′-GDT-3′ and 5′-GZT-3′

		rise (Å)	twist (deg)
d1	GC/AT	3.32 ± 0.26[a]	34.1 ± 6.0
		3.37[b]	32.6
d2	GC/DT	3.37 ± 0.31	32.1 ± 4.4
		3.42	31.9
d3	GC/ZT	3.51 ± 0.28	31.6 ± 3.6
		3.42	30.6
d1	AT/TA	3.35 ± 0.22	31.5 ± 2.4
		3.23	30.6
d2	DT/TD	3.36 ± 0.25	29.9 ± 2.7
		3.36	30.8
d3	ZT/TZ	3.36 ± 0.14	29.4 ± 2.1
		3.28	30.3

[a] The standard deviation is evaluated by taking into account the weight of each representative structure, which is the normalized population of the cluster. The values for rise and twist are obtained as weighted averages over the 10 representative structures for *d1*, *d2* and *d3*. [b] The values in the second row for each oligomer pertain to the average structures over 20 ns.

(the standard deviation also takes into account the weights of the representative structures), along with the values for the average structures. The largest differences in the rise amount to *ca.* 0.2 Å, which compare with the magnitude of the standard deviations sampled along the trajectories. Similarly, insertion of D and Z tends to decrease the twist by around 2 degrees, even though the magnitude of this change is lower than the standard deviation of this helical parameter.

Both major and minor grooves show similar fluctuations in the three duplexes (Figure 2). The fluctuation of the average width of major groove is in the range 12.15−14.83 Å (Δ = 2.68 Å), 12.55−14.14 Å (Δ = 1.59 Å) and 11.62−14.06 Å (Δ = 2.44 Å) for the *d1*, *d2* and *d3* oligomers, respectively. The corresponding values for the minor groove width are 6.10−7.90 Å (Δ = 1.80 Å), 7.05−7.90 Å (Δ = 0.85 Å) and 6.61−7.80 Å (Δ = 1.19 Å). Thus, these data reveal a reduced fluctuation for the *d2* duplex, which can be attributed to the stabilization afforded by the formation of the third hydrogen bond upon pairing between D and T. On the other hand, the largest fluctuations are found for the *d1* duplex, as expected from the reduction in stabilization afforded by H-bonding interactions of A compared to D and Z (Table 2). Note that the replacement of A with D and Z in the central portion of the dodecamer modifies the shape of helix, with particular reference to the minor groove width: in fact, the curves (Figure 2, right) for *d2* and *d3* do not show the typical well associated with A-rich tracts and lose the typical symmetry of A-rich central tracts. A similar trend was recently noted for other strategies of adenine replacement, with consequences on the electrostatic potential and protein−DNA binding.[25]

The analysis of the structural details of the duplexes suggest that, on average, the replacement of A by D or

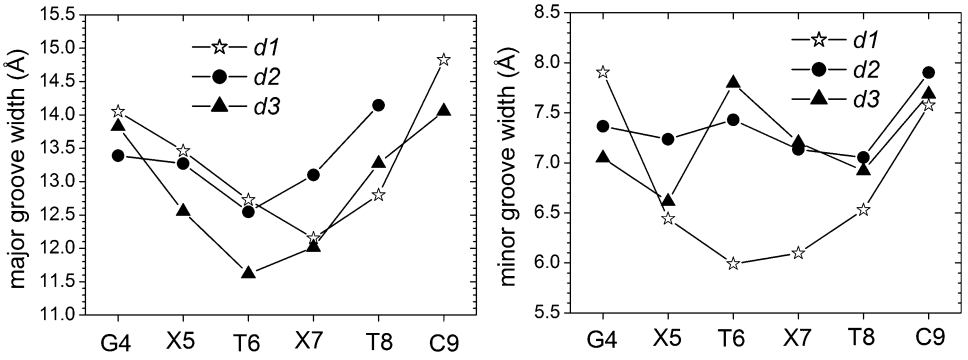

Figure 2. Plots of the major (left) and minor (right) groove widths in the central portion of the oligomers, as a function of the base-pair location along the sequence (G4 is on the 5′-ter). X = A, D, T in *d1*, *d2*, *d3*, respectively. These values have been computed as weighted averages over the 10 representative structures for each oligomer. The trends are similar for the grooves of the average structures and for time averages over the final 5 ns of the trajectories.

	HOMO-2	HOMO-1	HOMO	LUMO
$^{1}d1_{6}$	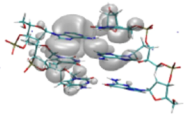 -7.57 eV	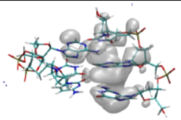 -7.14 eV	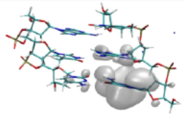 -6.68 eV	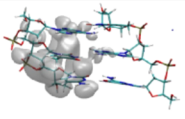 -0.42 eV
$^{2}d1_{0}$	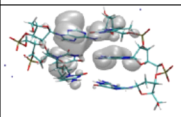 -7.39 eV	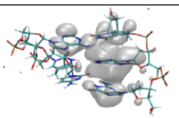 -7.07 eV	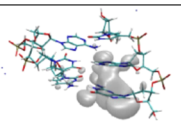 -6.78 eV	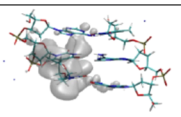 -0.39 eV
d1	-7.49 eV	-7.11 eV	-6.73 eV	-0.41 eV

Figure 3. Isodensity plots of electron orbitals around the HOMO–LUMO gap for the 5′-GAT-3′ trimers extracted from two of the most populated structures of *d1*, namely, $^{1}d1_{6}$ and $^{2}d1_{0}$. The energy of the electron level is indicated for each orbital, relative to the *vacuum* level. The weighted average of each electron level (populations in Supporting Information) over the two illustrated representative structures is reported in the bottom row.

	HOMO-2	HOMO-1	HOMO	LUMO
$^{0}d2_{3}$	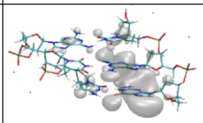 -6.81 eV	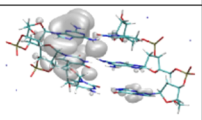 -6.75 eV	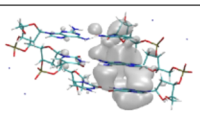 -6.53 eV	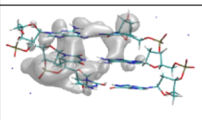 -0.26 eV
$^{1}d2_{4}$	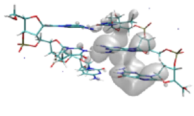 -6.85 eV	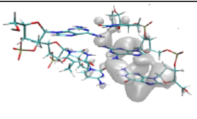 -6.64 eV	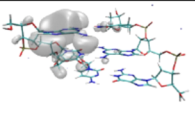 -6.60 eV	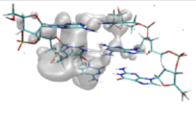 -0.43 e
$^{2}d2_{7}$	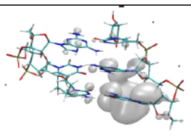 -6.81 eV	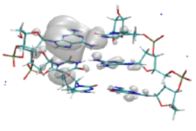 -6.67 eV	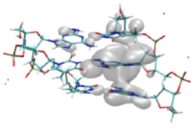 -6.33 eV	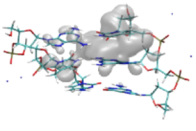 -0.38 eV
d2	-6.82 eV	-6.69 eV	-6.49 eV	-0.35 eV

Figure 4. Isodensity plots of electron orbitals around the HOMO–LUMO gap for the 5′-GDT-3′ trimers extracted from the three most populated (mp) structures of *d2*, namely, $^{0}d2_{3}$, $^{1}d2_{4}$ and $^{2}d2_{7}$. The energy of the electron level is indicated for each orbital, relative to the *vacuum* level. The weighted average of each electron level (populations in Supporting Information) over the three illustrated representative structures is reported in the bottom row.

TABLE 3. Calculated Energy Gaps between HOMO and LUMO and between HOMO and HOMO-1 for Trimers of Base Pairs Pruned from the Simulated Duplexes *d1*, *d2* and *d3*

	d1 5′-GAT-3′	*d2* 5′-GDT-3′	*d3* 5′-GZT-3′
	HOMO−LUMO gap (eV)		
value[a] of the average structure	6.52	6.28	6.43
weighted-average value[b] over mp structures of Figures 3−5	6.32	6.14	6.30
	$E_{HOMO} - E_{HOMO-1}$ (eV)		
value[a] of the average structure	0.40	0.19	0.22
weighted-average value[b] over mp structures of Figures 3−5	0.38	0.20	0.20

[a] From Figure S2, Supporting Information. [b] From the bottom values in Figures 3−5 .

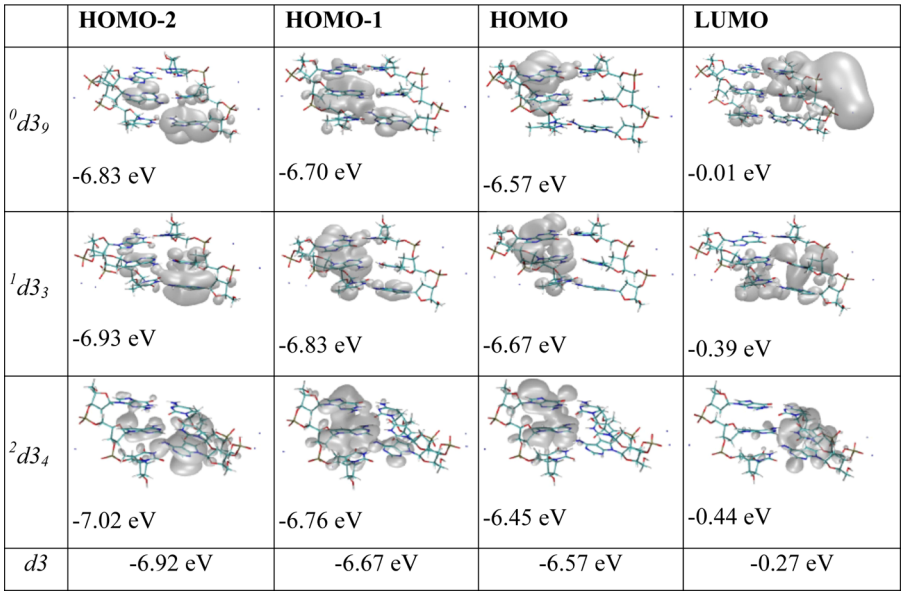

Figure 5. Isodensity plots of electron orbitals around the HOMO−LUMO gap for the 5′-GZT-3′ trimers extracted from the three most populated structures of *d3*, namely, $^0d3_9$, $^1d3_3$ and $^2d3_4$. The energy of the electron level is indicated for each orbital, relative to the *vacuum* level. The weighted average of each electron level (populations in Supporting Information) over the three illustrated representative structures is reported in the bottom row.

Z does not introduce significant alterations in the gross structural features of the duplex nor in the local parameters of the helical bases. Therefore, these findings support the reliability of the sampled structures to extract representative snapshots for electronic structure calculations (see below).

Ground-State Electronic Structure from DFT. We know from previous experience that the shape and order of electron orbitals in stacked dimers of Watson−Crick base pairs drastically depend on the sequence and on the details of the geometry, especially in the presence of large amounts of A−T pairs. Isosurface plots of the frontier orbitals are visualized in Figures 3−5 for the representative structures of the two most populated clusters of *d1* ($^1d1_6$ and $^2d1_0$) and of the three most populated clusters of *d2* ($^0d2_3$, $^1d2_4$ and $^2d2_7$) and *d3* ($^0d3_9$, $^1d3_3$ and $^2d3_4$). In agreement with existing computational data,[26−28] in the selected fragments 5′-GAT-3′, 5′-GDT-3′ and 5′-GZT-3′ the HOMO and HOMO-1 orbitals are localized on the purine bases (Figures 3−5). The shape and the energies of the molecular orbitals localized on the bases are affected by the substitution of A. In particular, the value of $\Delta E_{HOMO-LUMO}$ (Table 3) is not significantly modified by the replacement of A with D or Z along the sequence (less than 4%). Small variations are due to structural fluctuations associated with the presence of the water solvent and counterions. In contrast, we note a shrink in the separation between HOMO and HOMO-1 (Table 3; the abbreviation "mp" in Table 3 stands for "representative structure of the most populated clusters").

When A is replaced with D in duplex *d2*, among the most populated representative structures we observe only one case, $^1d2_4$ (Figure 4), in which HOMO and HOMO-1 are apparently inverted: actually, the tiny energy difference of 0.04 eV between them makes these two states practically degenerate. In all other cases, including averaged structures (Figure S2 in the Supporting Information), the HOMO orbital is always localized on D and G of the same strand, and the

TABLE 4. Computed Values of the Transfer Integral V_{IF} between the Adjacent Couples of Base Pairs in Each Representative Trimer[a]

		V_{IF}(GX) (eV)				V_{IF}(XT) (eV)			
	p_i ($d1_i$)	V_{IF}[b]	$^{wa}V_{IF}$	$^{mp}V_{IF}$	$^{as}V_{IF}$	V_{IF}	$^{wa}V_{IF}$	$^{mp}V_{IF}$	$^{as}V_{IF}$
d1 5′-GAT-3′ (X = A)	**0.120**	**0.039**	0.081 ± 0.070	**0.028**	0.042	**0.088**	0.097 ± 0.048	**0.098**	0.045
	0.074	0.161				0.089			
	0.148	**0.044**				**0.058**			
	0.115	0.054				0.112			
	0.055	0.044				0.026			
	0.112	0.218				0.188			
	0.145	**0.003**				**0.147**			
	0.058	0.007				0.097			
	0.091	0.140				0.066			
	0.083	0.137				0.032			
d2 5′-GDT-3′ (X = D)	0.104	0.006	0.052 ± 0.040	**0.042**	0.065	0.003	0.017 ± 0.015	**0.016**	0.002
	0.019	0.164				0.036			
	0.117	0.092				0.014			
	0.155	**0.025**				**0.009**			
	0.133	**0.072**				**0.008**			
	0.073	0.002				0.003			
	0.105	0.054				0.048			
	0.122	**0.033**				**0.033**			
	0.092	0.040				0.024			
	0.081	0.136				0.003			
d3 5′-GZT-3′ (X = Z)	0.080	0.015	0.043 ± 0.037	**0.028**	0.074	0.018	0.068 ± 0.041	**0.078**	0.062
	0.041	0.022				0.015			
	0.099	0.044				0.025			
	0.148	**0.018**				**0.033**			
	0.132	**0.069**				**0.084**			
	0.056	0.089				0.112			
	0.080	0.084				0.119			
	0.090	0.003				0.106			
	0.123	0.102				0.034			
	0.152	**0.002**				**0.116**			

[a] Results for the three most dynamically populated conformers for each sequence are identified in bold. The average transfer integrals ($^{wa}V_{IF}$) for the dimers of base pairs in each species and the corresponding standard deviations are also reported. [b] V_{IF} is the hybrid-DFT value of the transfer integral for each trimer pruned from the 10 most representative structures in the MD trajectories. $^{wa}V_{IF}$ is obtained for each duplex as a weighted average over all 10 values, with the population of the structure as the weight. $^{mp}V_{IF}$ is obtained for each duplex as a weighted average over the three most dynamically populated structures. $^{as}V_{IF}$ is the transfer integral value computed for the average structure over the final 5 ns of each 20-ns trajectory.

HOMO-1 orbital is localized on the D base of the opposite strand. The energy difference between HOMO and HOMO-1 in the sampled trimers reported in Figure 4 is 0.22 eV in $^{0}d2_3$, 0.04 eV in $^{1}d2_4$ and 0.34 eV in $^{2}d2_7$. The weighted average of 0.20 eV is practically identical to the value of 0.19 eV that pertains to the trimer pruned from the average structure of the duplex *d2* (see Supporting Information).

When A is replaced with Z in duplex *d3*, all the sampled structures show the HOMO localized on Z and G of the same strand and the HOMO-1 localized on all the purine nucleobases Z and G of both strands. The energy difference between HOMO and HOMO-1 in Figure 5 is 0.13, 0.16, and 0.31 eV for $^{0}d3_9$, $^{1}d3_3$, and $^{0}d3_9$, respectively, with a weighted average of 0.20 eV, which is practically identical to the value of 0.22 eV that pertains to the trimer pruned from the average structure of the duplex *d3* (see Supporting Information).

To summarize, we observe shifts of the energy levels for each sequence, which highlights the importance of examining various conformations among the most populated from the dynamical runs. Furthermore, the chemical changes induce the redistribution of charge densities in frontier orbitals, which in turn may affect the $\pi-\pi$ coupling and charge transfer capabilities. In the next paragraph, the 10 representative structures from each trajectory are considered, in order to obtain the charge transfer parameters for the pruned trimers.

Transfer Integrals from Hybrid-DFT Computation. Charge transfer integrals between adjacent base pairs were computed for 5′-GAT-3′, 5′-GDT-3′ and 5′-GZT-3′ trimers pruned from the 10 representative structures obtained from the trajectories of duplexes *d1*, *d2* and *d3*. The results are summarized in Table 4, and the same data are visualized in Figure 6. The much smaller

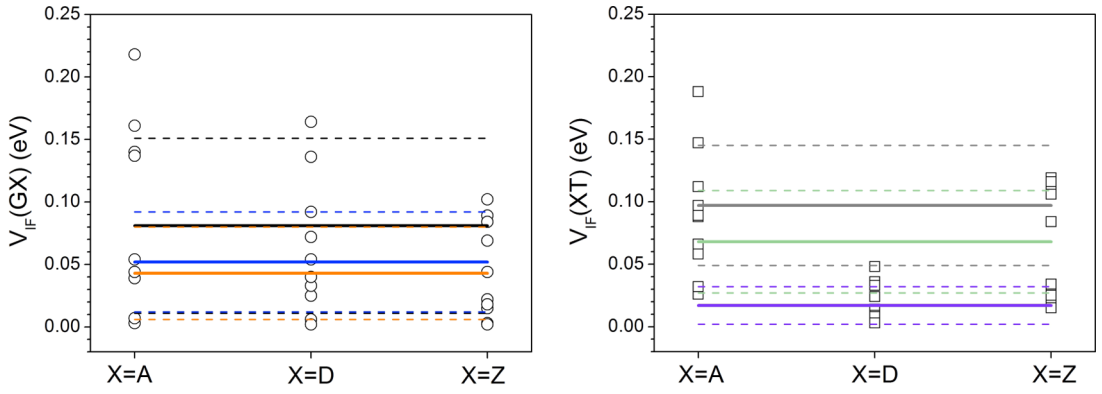

Figure 6. Values of the transfer integrals V_{IF}(GX) and V_{IF}(XT), as from Table 4, are plotted as open circles and squares on the left and right, respectively. The horizontal thick solid lines represent $^{wa}V_{IF}$(GA) (black), $^{wa}V_{IF}$(GD) (blue), $^{wa}V_{IF}$(GZ) (orange), $^{wa}V_{IF}$(AT) (gray), $^{wa}V_{IF}$(DT) (violet), $^{wa}V_{IF}$(ZT) (green). The dashed lines of the respective color marks $^{wa}V_{IF}$(GX) + σ(GX) and $^{wa}V_{IF}$(GX) − σ(GX) (left), $^{wa}V_{IF}$(XT) + σ(XT) and $^{wa}V_{IF}$(XT) − σ(XT) (right), where the symbol σ stands for the weighted standard deviation (Table 4). Values of the Pearson correlation between the transfer integrals and the rise and twist for the sets of 10 representative structures are very small (between 0.1 and 0.5), indicating no obvious correlation between these quantities.

electronic couplings between the edges of the trimers (V_{GT}) are reported in the Supporting Information.

We note a significant effect of structural fluctuations on the transfer integrals. In fact, the standard deviation is about 80−85% of the weighted-average transfer integral in all three sequences, which amounts to a coherence parameter significantly smaller than unity.[29,30] Note that the reported standard deviations are much larger than the computational error in each evaluation, and thus essentially reflect the change in the transfer integral with the nuclear conformation, which embeds a coherence parameter.

We aim at detecting if the replacement of A with D and/or Z leads to an increase of transfer integrals that can be correlated to the measurements of higher charge transfer rates in D- and Z-containing sequences.[8−10]

If we consider the weighted average using all the 10 representative conformers for each duplex, the data in Table 4 indicates that both $^{wa}V_{IF}$(GX) and $^{wa}V_{IF}$(XT) decrease with these transformations. However, the ranges of values for the different geometries widely overlap. Therefore, according to the presented data, the overall hole transfer rate appears not to be sensitive to the changes in the electronic couplings caused in the pruned trimer sequences by the adenine derivatives. If we consider the weighted average using only the three most populated structures among the 10 representative conformers for each sequence, we see that $^{mp}V_{IF}$(GX) increases when A is replaced with D and is unchanged when A is replaced with Z, while $^{mp}V_{IF}$(XT) decreases as a consequence of each substitution.

Finally, if we consider the values of V_{IF} obtained for the trimers pruned from each average structure, we register an increase of $^{as}V_{IF}$(GX) after both modifications (*d1* → *d2*, *d1* → *d3*), while $^{as}V_{IF}$(XT) increases when *d1* → *d3* and decreases when *d1* → *d2*. These results, compared with the above structural analysis, show that for the systems under study the average transfer integral under the Condon approximation[31] is not a significant kinetic parameter, although the Condon approximation may be applicable over limited portions of the conformational space.[32]

We searched for trends in the behavior of the transfer integrals as a function of the structural parameters. In particular, we inspected possible correlations between the values of V_{IF} for the 10 representative structures for each sequence and the corresponding inter-bp structural parameters (shift, slide, rise, tilt, roll, twist). Interestingly, we did not find any reasonable correlation between V_{IF}(GX,XT) and such descriptors, but we detected a negative correlation between V_{IF}(XT) and the minimum interstrand atomic distance. Indeed, the Pearson correlation coefficient for the latter is −0.87 for *d1* and −0.75 for *d2* and *d3*. At odds, the Pearson correlation coefficient for either V_{IF}(GX) or V_{IF}(XT) and the helical inter-bp values are always smaller than 0.5 and with alternating signs, with a couple of fortuitous exceptions that do not involve the rise.

Overall, the changes in the values of the transfer integrals obtained with these chemical alterations of the adenine base are not able alone to explain the experimental results, which report an increase of transfer rates with both substitutions. We argue that this is not necessarily a negative result and actually gives us insights into the physicochemical mechanisms in these systems. Different reasons can explain this apparent discrepancy. (1) Despite the performed computational tests, use of CDFT with more diffuse functions in the basis set (still not allowed, *e.g.*, by NWChem) is desirable. Moreover, future investigation using different amounts of exact exchange in the density functional may help to rule out effects of large electron self-interaction errors.[33,34] (2) The large fluctuations in the transfer integral values obtained in this work for different representative structures point out the need to explore more configurations, with a longer dynamics and/or a finer sampling. (3) We should remember at this point that we did not simulate exactly the experimental

sequences, and a viable hypothesis is that sequence effects emerge to determine the efficiency of the considered chemical transformations for what concerns the rate of charge transfer. (4) It is possible that the electronic coupling factor alone in this case is not representative of the complex charge transfer phenomenon, because the role of the reorganization energy and collective modes is important.

As a matter of fact, our results suggest that for the systems investigated in this work as a model for charge transport through DNA duplexes, the transfer integrals are not sufficient to explain the observed trends: also the kinetics of the hole excited states is relevant. This conclusion of the present work provides specific useful information on the systems under study, while it is not necessarily a general result for DNA but depends on the sequence and on the base chemistry.

CONCLUSIONS

We undertook this theoretical work to explain the experimental data on charge transfer by Majima's group,[9,10] in terms of electronic structure and conformational fluctuations. We find seemingly contradictory results. In what follows we consider the reasons for the apparent discrepancy.

First of all, we noted at the beginning that the specific adenine modifications with D and Z were chosen because of the lower ionization potential of such derivatives, thus making them more similar to guanine, which is known to be an effective hole transfer mediator. We find indeed that D and Z have a lower ionization potential than A, by 0.24 and 0.16 eV, respectively (from the data in the bottom rows of Figures 3−5). This outcome of DFT is in line with the experimental indications. Yet, we find that larger ionization potentials do not necessarily correspond to larger electronic couplings.

The process of electron/hole transfer depends in fact on a peculiar balance of electronic (both ground and excited states) and vibronic effects, according to Marcus−Hush−Jortner theory.[35−37] Intuitively, one would expect that larger effective electronic couplings yield faster electronic motion, but a complete treatment goes beyond the electronic coupling factors.

The trends that we find in the transfer integrals are not surprising: namely, the larger rise and overall major orbital charge localization (HOMO and HOMO-1) in the sequences with D and Z than in the sequence with A would indeed point to a negative effect on the transfer integrals, although we could not find a strict correlation between rise and V_{IF} for each sequence. Then, how can we reconcile our computational findings on nonincreasing transfer integrals with the experimental evidence of increasing transfer rates for the D- and Z-containing sequences? We already noted above some possible reasons of the apparent discrepancy: sequence effects, intrinsic computational errors, statistical sampling limitations. In our approach, we have made a big effort to account for structural effects in a classical regime. However, this is not the whole story: slow motions can be traps for configurations particularly suitable for fast charge transfer, and the reorganization energy can reverse the trends indicated by the electronic term. These arguments are not necessarily valid in general for any DNA molecules, but care should be taken in using the sole transfer integrals to predict charge transfer through DNA.

As a matter of fact, the positive conclusions of our study are as follows: (i) we propose a viable and effective multilevel strategy to describe structural effects in electronic problems for biological systems; (ii) we find that structural fluctuations are indeed important in determining the electronic structure parameters; (iii) we point out a sensitivity of the transfer integral in the central portion of the DNA oligomers to interstrand atomic distances; (iv) we find that the replacement of adenine with D and Z in the simulated sequences has remarkable consequences on the electronic structure and transfer integrals; (v) we argue on the need for further theoretical/computational development toward a predictive role in problems of charge transfer in biological systems.

MATERIALS AND METHODS

In order to investigate the effect of incorporating Z and D in a DNA duplex, we have performed electronic structure calculations for structural fragments extracted from classical MD trajectories, which allow us to take into account the effect of thermal fluctuations associated with the inherent flexibility of the duplex and with the presence of the water solvent and counterions.

Materials. Starting from the duplexes that were targeted by charge transfer measurements,[9] the effect of replacing A by Z and D was examined by using the central tract of the Dickerson dodecamer[38] d(CGCGAATTCGCG), named after R.E. Dickerson, as template. Accordingly, the central segment AATT was replaced by the alternative sequence XTXT (with X = A, Z, D), which mimics one of the sequence motifs examined experimentally by Majima and co-workers,[9,10] thus leading to the three duplexes shown in Figure 1. Furthermore, this choice is motivated by the fact that the Dickerson dodecamer has been extensively used as a benchmark for classical MD simulations,[39−41] thus enabling the analysis of the structural properties of the modified duplexes. The rationale behind the definition of the Dickerson-like duplexes is that, even if they are not identical to the experimental sequences and therefore cannot yield a one-to-one comparison of computed and measured data, they are optimal reference systems to examine the impact of replacing A by Z and D on the structural and electronic properties of the duplex.

The starting configuration for each oligomer was constructed on the basis of the sequence with NAB[42] using canonical B-DNA parameters.

Development of Force Field Parameters (AMBER) for Deaza-Adenine and Diaminopurine. MD simulations were performed using the parmbsc0 version of the AMBER force field.[39] For the sake of

consistency in electronic structure calculations (see below), force field parameters for the nonstandard bases Z and D were determined based on *ab initio* DFT calculations using the Becke functional with partial exact exchange (BHH[43]) and the cc-pVTZ basis set.[44,45] RESP charges were derived for the optimized structures of the Z and D bases at the BHH/cc-pVTZ level with the Gaussian09 code, and standard *parmbsc0* were used for A (Table S1 in the Supporting Information). Missing bond and angle parameters were built using the tools of the AMBER10 package,[46] starting from the optimized BHH/cc-pVTZ geometries.

The force field parameters were tested by comparison of the interaction energies of H-bonded base pairs (Figure 1c) and stacked dimers (Figure 1d) computed at different levels of theory, including classical molecular mechanics (MM) and quantum electronic structure calculations, as suggested elsewhere.[20,22,23,47] To this end, the H-bonding interaction energies of A−T, D−T and Z−T pairs (Figure 1c) were obtained from calculations performed at the BHH/cc-pVTZ, MP2/6-31G(d) and parmbsc0 levels.[20,47] The geometries of the optimized single bases were superposed to the base-pair structures of the empirical DNA-duplexes created with NAB.[42] The base pairs were then fully relaxed by BHH/cc-pVTZ calculations including BSSE[48,49] corrections, and the optimized geometries were subsequently used in single-point energy calculations.

Stacking interaction energies were determined using the geometries of the individual bases optimized at the MP2/6-31G(d) level. The optimized geometries were then superposed to the corresponding units in a stacked dimer using standard geometrical parameters for a canonical B-DNA duplex, without further dimer relaxation in the gas phase.[22,23] Single-point BSSE calculations of the formation energies were performed at the MP2/6-31G(d,0.25) level. Let us note that this procedure has been shown to provide reliable estimates of the stacking energies for nucleic acid basis at a reasonable cost.[25] Furthermore, stacking energies were also determined using the M062X functional and the 6-31+G(d) basis and from MM calculations.

Molecular Dynamics Simulations. Classical MD simulations with explicit solvent molecules and counterions for the three DNA dodecamers were carried out to benchmark the novel force field parameters and to yield trajectories that encompass the dynamical fluctuations of the selected dodecamer sequences. Runs of 20 ns of MD for the duplexes *d1*, *d2* and *d3* (Figure 1b) were performed using the *parmbsc0* force field in the AMBER10 suite of codes.[46]

Each simulation system was prepared by immersing the NAB-constructed DNA oligomer in explicit solvent. Specifically, an octahedral box was generated, by adding a buffer layer (12 Å in each spatial direction) of TIP3P water molecules with standard hydration rules.[50] Twenty-two Na^+ counterions were added in the simulation box to ensure the neutrality of the whole system: such ions were placed according to the electronegativity map yielded by Poisson−Boltzmann calculations.[51]

Simulations were performed in the isothermic isobaric ensemble (P = 1 atm, T = 300 K). Periodic boundary conditions and the Particle−Mesh−Ewald algoritm[52] were used. A 2 fs integration time step was used, and all bonds involving hydrogen atoms were constrained with the SHAKE algorithm.[53] The simulation protocol for each oligomer included an equilibration phase constituted of various steps of optimization of atomic coordinates and restrained finite-temperature dynamics during which the restraints on DNA atoms were gradually weakened and eventually released, according to a previously reported procedure[54−56] (see details in the Supporting Information). At the end of the equilibration the trajectories were stable in terms of density, temperature, potential energy and other macroscopic properties. The equilibration phase was followed by unrestrained dynamics at room temperature for 20 ns, starting from the equilibrated structure and collecting the coordinates every 1 ps. The backbone root-mean-square deviation (RMSD) for each of the three duplexes relative to the respective equilibrated structure was computed at every instant along the whole time evolution: the RMSD analysis supported the stability of trajectories over time (Figure S1 in the Supporting Information).

To analyze the structural impact of the replacement of A with Z and D, we performed additional conformational sampling (sorting and averaging of the trajectories) of the three simulated systems to select a few representative structures suitable for DFT calculations that would embody dynamical effects. For each trajectory, the average structure was evaluated during the entire 20 ns MD run. Clustering with a simple means algorithm[57] was applied during the last 5 ns of the 20 ns MD run, extracting 10 representative structures for each trajectory: we will label such representative structures as ${}^hdM_k$, where M = 1, 2, 3 indicates the duplex, k = 0, ..., 9 is an index that is associated with sequential structures extracted by the sorting algorithm, h = 0, ..., 9 is an index for the order of the representative structures by decreasing population (h = 0 pertains to the most populated structure). Analysis of the helical parameters of such representative structures was done with CURVES+.[58] A double-stranded trimer (5′-GAT-3′, 5′-GDT-3′ and 5′-GZT-3′) was pruned from each representative structure and from the average structure.

Quantum Ground-State Electronic Structure of Representative Trimers Calculations by DFT. Calculations of the ground-state electronic structure to inquire on the nature of the energy levels and wave functions of the trimers were performed at the BHH/cc-pVTZ level of theory. Solvent effects were also included in the electronic properties through the PCM continuum model,[59] to correctly describe the screening effects of the solvent on backbone-localized states that fall around the HOMO−LUMO gap in the gas-phase. This was done on both the average MD structure and the most representative structures.

Transfer Integrals between Base Pairs in Representative Trimers by DFT. We computed the electronic coupling between each couple of base pairs in the trimer by using the idea of constrained charge (specifically, hole) density in a portion of the system,[60,61] as implemented in the NWChem computational chemistry package.[62−64] Once two base pairs, denoted by *I* and *J*, are picked as the donor and acceptor groups for a given hole transfer process, the third base pair, *K*, represents the neighbor environment that affects the electronic coupling between *I* and *J*. This approximate picture can be used, *e.g.*, to calculate the two-state transfer integrals involved in the formulation of the transfer integral for forward electron superexchange through the trimer starting from localization of the electron hole in the GC unit. Clearly, in general, one may also need to consider the nearest neighbor bases to the trimer edges. Note also that *K* acts as a bridge if it is the central base pair. The charge-transfer integrals between adjacent nucleobase pairs are key quantities in establishing superexchange couplings and thus related rates.

Transfer integrals are obtained as follows. (i) By means of constrained density functional theory (CDFT)[62,63] we calculate a constrained ground state with the excess charge localized in the *I*−*J* subsystem, $|\psi_{IJ}\rangle$, and the diabatic states $|\psi_I\rangle$ and $|\psi_J\rangle$ with the electron hole in *I* and *J*, respectively. (ii) On the basis of the two-state approximation, $|\psi_{IJ}\rangle$ is written as the linear combination $a_I|\psi_I\rangle + a_J|\psi_J\rangle$, and the transfer integral is as follows:[65,66]

$$V_{IJ} = \left| \frac{A_I A_J}{A_I^2 - A_J^2} \Delta E_{IJ} \left(1 - \frac{A_I^2 + A_J^2}{2A_I A_J} S_{IJ} \right) \frac{1}{1 - S_{IJ}^2} \right| \qquad (1)$$

In eq 1 ΔE_{JK} is the energy difference between the two diabatic states, $S_{IJ} = \langle\psi_I|\psi_J\rangle$, $A_I \equiv \langle\psi_I|\psi_{IJ}\rangle = a_I + a_J S_{IJ}$, and A_J is similarly defined exchanging *I* with *J*. eq 1 can be also used to compute the direct coupling between the edge base pairs in the trimers (see Supporting Information).

After the tests detailed in the Supporting Information, our DFT method of choice to compute the electronic structure parameters in eq 1 was to use (i) the hybrid exchange-correlation functional derived from the adiabatic connection method[67] with coefficients given by the Becke B1 convention[68] and 50% of exchange of the exact (Hartree−Fock) form based on Kohn−Sham orbitals; (ii) the 6-311G** basis set for H and C atoms and the 6-311+G* basis set for N and O atoms. The transfer integrals are greatly sensitive to the electronic structure, and in particular to electron exchange-correlation effects: hence, the details of the DFT computation were specifically optimized through stringent tests.

Our method rests on full-electron computation of Slater determinants of molecular orbitals for the overall trimeric system. Moreover, the two-state approximation for the three

CDFT states defined above has been assessed computationally: The norm of $|\psi_{IJ}\rangle$, given by $(a_I^2 + a_J^2 + 2a_Ia_JS_{IJ})^{1/2}$ for the real wave functions produced by the NWChem program, was usually between 0.996 and unity, and never less than 0.990. Therefore, the method does not suffer from typical issues related to use of monomer orbital basis and site energies.[69]

Conflict of Interest: The authors declare no competing financial interest.

Acknowledgment. This work was funded by the European Commission through Project "DNA-Nanodevices" (Contract FP6-029192), by the ESF through the COST Action MP0802, by the Italian Institute of Technology through Project MOPROSURF and the Computational Platform, and by Fondazione Cassa di Risparmio di Modena through Progetto Internazionalizzazione 2011. The ISCRA staff at CINECA (Bologna, Italy) is acknowledged for computational facilities and technical support. A.M. thanks Abraham Nitzan and David Beratan, and acknowledges support from the Israel Science Foundation, the European Science Council (FP7/ERC Grant Number 226628), and NIH (Award Number GM071628). Moreover, A.M. acknowledges computational support from Tel Aviv University. G.B. acknowledges "HPC-Europa2" (Project Ref 2010/361) and BSC (Barcelona Supercomputing Center) for computational resources and technical support. G.B. further acknowledges the Center for Nanophase Materials Sciences (CNMS): a portion of this research was conducted at CNMS, which is sponsored at Oak Ridge National Laboratory by the Scientific User Facilities Division, Office of Basic Energy Sciences, U.S. Department of Energy. Facilities of the National Energy Research Scientific Computing Center (NERSC), which is supported by the Office of Science of the U.S. Department of Energy under Contract No. DE-AC02-05CH11231, are also acknowledged.

Supporting Information Available: Details on the molecular dynamics simulation protocols, in particular for the minimization-equilibration phase. Figure S1 reports some results of the MD trajectories (three-dimensional structures and root-mean-square deviations). Figure S2 reports isodensity plots of frontier orbitals for trimers extracted from the average dynamical structures of *d1*, *d2* and *d3*. Table S1 reports the computed RESP charges for A, D and Z. Table S2 compiles details of the most representative structures from the clustering analysis. Tables S3 and S4, accompanied by related text, describe results of tests to determine the level of accuracy in transfer integral computations. These materials are available free of charge *via* the Internet at http://pubs.acs.org.

REFERENCES AND NOTES

1. Joachim, C.; Ratner, M. A. Molecular Electronics: Some Views on Transport Junctions and Beyond. *Proc. Natl. Acad. Sci. U. S. A.* **2005**, *102*, 8801–8808.
2. Porath, D.; Cuniberti, G.; Di Felice, R. Charge Transport in DNA-Based Devices. *Top. Curr. Chem.* **2004**, *237*, 183–227.
3. Kasumov, A. Y.; Klinov, D. V.; Roche, P. E.; Gueron, S.; Bouchiat, H. Thickness and Low-Temperature Conductivity of DNA Molecules. *Appl. Phys. Lett.* **2004**, *84*, 1007–1009.
4. Cohen, H.; Nogues, C.; Naaman, R.; Porath, D. Direct Measurement of Electrical Transport through Single DNA Molecules of Complex Sequence. *Proc. Natl. Acad. Sci. U. S. A.* **2005**, *102*, 11589–11593.
5. Xu, B. Q.; Zhang, P. M.; Li, X. L.; Tao, N. J. Direct Conductance Measurement of Single DNA Molecules in Aqueous Solution. *Nano Lett.* **2004**, *4*, 1105–1108.
6. Kang, N.; Erbe, A.; Scheer, E. Electrical Characterization of DNA in Mechanically Controlled Break-Junctions. *New J. Phys.* **2008**, *10*, 023030.
7. Cohen, H.; Nogues, C.; Ullien, D.; Daube, S.; Naaman, R.; Porath, D. Electrical Characterization of Self-Assembled Single- and Double-Stranded DNA Monolayers Using Conductive AFM. *Faraday Discuss.* **2006**, *131*, 367–376.
8. Takada, T.; Kawai, K.; Fujitsuka, M.; Majima, T. Contributions of the Distance-Dependent Reorganization Energy and Proton-Transfer to the Hole-Transfer Process in DNA. *Chem.—Eur. J.* **2005**, *11*, 3835–3842.
9. Kawai, K.; Kodera, H.; Osakada, Y.; Majima, T. Sequence-Independent and Rapid Long-Range Charge Transfer through DNA. *Nat. Chem.* **2009**, *1*, 156–159.
10. Kawai, K.; Kodera, H.; Majima, T. Long-Range Charge Transfer through DNA by Replacing Adenine with Diaminopurine. *J. Am. Chem. Soc.* **2010**, *132*, 627–630.
11. Nakatani, K.; Dohno, C.; Saito, I. Modulation of DNA-Mediated Hole-Transport Efficiency by Changing Superexchange Electronic Interaction. *J. Am. Chem. Soc.* **2000**, *122*, 5893–5894.
12. Kelley, S. O.; Barton, J. K. Electron Transfer Between Bases in Double Helical DNA. *Science* **1999**, *283*, 375–381.
13. Voityuk, A. A.; Rosch, N. Quantum Chemical Modeling of Electron Hole Transfer through π Stacks of Normal and Modified Pairs of Nucleobases. *J. Phys. Chem. B* **2002**, *106*, 3013–3018.
14. Bixon, M.; Jortner, J. Charge Transport in DNA *via* Thermally Induced Hopping. *J. Am. Chem. Soc.* **2001**, *123*, 12556–12567.
15. Troisi, A.; Orlandi, G. Hole Migration in DNA: A Theoretical Analysis of the Role of Structural Fluctuations. *J. Phys. Chem. B* **2002**, *106*, 2093–2101.
16. Kubar, T.; Elstner, M. What Governs the Charge Transfer in DNA? The Role of DNA Conformation and Environment. *J. Phys. Chem. B* **2008**, *112*, 8788–8798.
17. Tonzani, S.; Schatz, G. C. Electronic Excitations and Spectra in Single-Stranded DNA. *J. Am. Chem. Soc.* **2008**, *130*, 7607–7612.
18. Lee, M. H.; Brancolini, G.; Gutierrez, R.; Di Felice, R.; Cuniberti, G. Probing Charge Transport in Oxidatively Damaged DNA Sequences under the Influence of Structural Fluctuations. *J. Phys. Chem. B* **2012**, *116*, 10977–10985.
19. Renaud, N.; Berlin, Y. A.; Lewis, F. D.; Ratner, M. A. Between Superexchange and Hopping: An Intermediate Charge-Transfer Mechanism in Poly(A)-Poly(T) DNA Hairpins. *J. Am. Chem. Soc.* **2013**, *135*, 3953–3963.
20. Blas, J. R.; Luque, F. J.; Orozco, M. Unique Tautomeric Properties of Isoguanine. *J. Am. Chem. Soc.* **2004**, *126*, 154–164.
21. Huertas, O.; Blas, J. R.; Soteras, I.; Orozco, M.; Luque, F. J. Benzoderivatives of Nucleic Acid Bases as Modified DNA Building Blocks. *J. Phys. Chem. A* **2006**, *110*, 510–518.
22. Sponer, J.; Jurecka, P.; Marchan, I.; Luque, F. J.; Orozco, M.; Hobza, P. Nature of Base Stacking: Reference Quantum-Chemical Stacking Energies in Ten Unique B-DNA Base-Pair Steps. *Chem.—Eur. J.* **2006**, *12*, 2854–2865.
23. Alhambra, C.; Luque, F. J.; Gago, F.; Orozco, M. *Ab Initio* Study of Stacking Interactions in A- and B-DNA. *J. Phys. Chem. B* **1997**, *101*, 3846–3853.
24. Hobza, P.; Sponer, J.; Polasek, M. H-Bonded and Stacked DNA-Base Pairs: Cytosine Dimer. An *Ab Initio* Second-Order Moller-Plesset Study. *J. Am. Chem. Soc.* **1995**, *117*, 792–798.
25. Hancock, S. P.; Ghane, T.; Cascio, D.; Rohs, R.; Di Felice, R.; Johnson, R. C. Control of DNA Minor Groove Width and Fis Protein Binding by the Purine 2-Amino Group. *Nucleic Acids Res.* **2013**, *41*, 6750–6760.
26. Di Felice, R.; Calzolari, A.; Zhang, H. Towards Metalated DNA-Based Structures. *Nanotechnology* **2004**, *15*, 1256–1263.
27. Brancolini, G.; Di Felice, R. Electronic Properties of Metal-Modified DNA Base Pairs. *J. Phys. Chem. B* **2008**, *112*, 14281–14290.
28. de Pablo, P. J.; Moreno-Herrero, F.; Colchero, J.; Gomez-Herrero, J.; Herrero, P.; Baro, A. M.; Ordejon, P.; Soler, J. M.; Artacho, E. Absence of dc-Conductivity in Lambda-DNA. *Phys. Rev. Lett.* **2000**, *85*, 4992–4995.
29. Balabin, I. A.; Onuchic, J. N. Dynamically Controlled Protein Tunneling Paths in Photosynthetic Reaction Centers. *Science* **2000**, *290*, 114–117.
30. Prytkova, T. R.; Kurnikov, I. V.; Beratan, D. N. Coupling Coherence Distinguishes Structure Sensitivity in Protein Electron Transfer. *Science* **2007**, *315*, 622–625.
31. Kuznetsov, A. M.; Ulstrup, J. Simple Schemes in Chemical Electron Transfer Formalism beyond Single-Mode Quadratic Forms: Environmental Vibrational Dispersion and Anharmonic Nuclear Motion. *Phys. Chem. Chem. Phys.* **1999**, *1*, 5587–5592.

32. Migliore, A. Nonorthogonality Problem and Effective Electronic Coupling Calculation: Application to Charge Transfer in pi-Stacks Relevant to Biochemistry and Molecular Electronics. *J. Chem. Theory Comput.* **2011**, *7*, 1712–1725.
33. Migliore, A.; Corni, S.; Varsano, D.; Klein, M. L.; Di Felice, R. First Principles Effective Electronic Couplings for Hole Transfer in Natural and Size-Expanded DNA. *J. Phys. Chem. B* **2009**, *113*, 9402–9415.
34. Tang, X. D.; Liao, Y.; Gao, H. Z.; Geng, Y.; Su, Z. M. Theoretical Study of the Bridging Effect on the Charge Carrier Transport Properties of Cyclooctatetrathiophene and its Derivatives. *J. Mater. Chem.* **2012**, *22*, 6907–6918.
35. Marcus, R. A.; Sutin, N. Electron Transfers in Chemistry and Biology. *Biochim. Biophys. Acta* **1985**, *811*, 265–322.
36. Hush, N. S. Adiabatic Rate Processes at Electrodes .1. Energy-Charge Relationships. *J. Chem. Phys.* **1958**, *28*, 962–972.
37. Jortner, J. Temperature-Dependent Activation-Energy for Electron-Transfer between Biological Molecules. *J. Chem. Phys.* **1976**, *64*, 4860–4867.
38. Drew, H. R.; Wing, R. M.; Takano, T.; Broka, C.; Tanaka, S.; Itakura, K.; Dickerson, R. E. Structure of a B-DNA Dodecamer: Conformation and Dynamics. *Proc. Natl. Acad. Sci. U. S. A.* **1981**, *78*, 2179–2183.
39. Perez, A.; Marchan, I.; Svozil, D.; Sponer, J.; Cheatham, T. E.; Laughton, C. A.; Orozco, M. Refinenement of the AMBER Force Field for Nucleic Acids: Improving the Description of Alpha/Gamma Conformers. *Biophys. J.* **2007**, *92*, 3817–3829.
40. Perez, A.; Luque, F. J.; Orozco, M. Frontiers in Molecular Dynamics Simulations of DNA. *Acc. Chem. Res.* **2012**, *45*, 196–205.
41. Ricci, C. G.; de Andrade, A. S. C.; Mottin, M.; Netz, P. A. Molecular Dynamics of DNA: Comparison of Force Fields and Terminal Nucleotide Definitions. *J. Phys. Chem. B* **2010**, *114*, 9882–9893.
42. Macke, T. J.; Case, D. A. Modeling Unusual Nucleic Acid Structures. *ACS Symp. Ser.* **1998**, *682*, 379–393.
43. Becke, A. D. A New Mixing of Hartree-Fock and Local Density-Functional Theories. *J. Chem. Phys.* **1993**, *98*, 1372–1377.
44. Wilson, A. K.; vanMourik, T.; Dunning, T. H. Gaussian Basis Sets for Use in Correlated Molecular Calculations .VI. Sextuple Zeta Correlation Consistent Basis Sets for Boron through Neon. *J. Mol. Struct.: THEOCHEM* **1996**, *388*, 339–349.
45. Dunning, T. H. Gaussian-Basis Sets for Use in Correlated Molecular Calculations .1. The Atoms Boron through Neon and Hydrogen. *J. Chem. Phys.* **1989**, *90*, 1007–1023.
46. Case, D. A.; Cheatham, T. E.; Darden, T.; Gohlke, H.; Luo, R.; Merz, K. M.; Onufriev, A.; Simmerling, C.; Wang, B.; Woods, R. J. The Amber Biomolecular Simulation Programs. *J. Comput. Chem.* **2005**, *26*, 1668–1688.
47. Sponer, J. E.; Vazquez-Mayagoitia, A.; Sumpter, B. G.; Leszczynski, J.; Sponer, J.; Otyepka, M.; Banas, P.; Fuentes-Cabrera, M. Theoretical Studies on the Intermolecular Interactions of Potentially Primordial Base-Pair Analogues. *Chem.—Eur. J.* **2010**, *16*, 3057–3065.
48. Jansen, H. B.; Ros, P. Non-Empirical Molecular Orbital Calculations on the Protonation of Carbon Monoxide. *Chem. Phys. Lett.* **1969**, *3*, 140–143.
49. Liu, B.; Mclean, A. D. Accurate Calculation of Attractive Interaction of Two Ground-State Helium-Atoms. *J. Chem. Phys.* **1973**, *59*, 4557–4558.
50. Pearlman, D. A.; Case, D. A.; Caldwell, J. W.; Ross, W. S.; Cheatham, T. E.; Debolt, S.; Ferguson, D.; Seibel, G.; Kollman, P. Amber, a Package of Computer Programs for Applying Molecular Mechanics, Normal Mode Analysis, Molecular Dynamics and Free Energy Calculations to Simulate the Structural and Energetic Properties of Molecules. *Comput. Phys. Commun.* **1995**, *91*, 1–41.
51. Shields, G. C.; Laughton, C. A.; Orozco, M. Molecular Dynamics Simulations of the d(T·A·T) Triple Helix. *J. Am. Chem. Soc.* **1997**, *119*, 7463–7469.
52. Essmann, U.; Perera, L.; Berkowitz, M. L.; Darden, T.; Lee, H.; Pedersen, L. G. A Smooth Particle Mesh Ewald Method. *J. Chem. Phys.* **1995**, *103*, 8577–8593.
53. Ryckaert, J. P.; Ciccotti, G.; Berendsen, H. J. C. Numerical Integration of Cartesian Equations of Motion of a System with Constraints: Molecular Dynamics of N-Alkanes. *J. Comput. Phys.* **1977**, *23*, 327–341.
54. Soliva, R.; Sherer, E.; Luque, F. J.; Laughton, C. A.; Orozco, M. Molecular Dynamics Simulations of PNA·DNA and PNA·RNA duplexes in Aqueous Solution. *J. Am. Chem. Soc.* **2000**, *122*, 5997–6008.
55. Spector, T. I.; Cheatham, T. E.; Kollman, P. A. Unrestrained Molecular Dynamics of Photodamaged DNA in Aqueous Solution. *J. Am. Chem. Soc.* **1997**, *119*, 7095–7104.
56. Soliva, R.; Garcia, R. G.; Blas, J. R.; Eritja, R.; Asensio, J. L.; Gonzalez, C.; Luque, F. J.; Orozco, M. DNA-Triplex Stabilizing Properties of 8-Aminoguanine. *Nucleic Acids Res.* **2000**, *28*, 4531–4539.
57. Shao, J. Y.; Tanner, S. W.; Thompson, N.; Cheatham, T. E. Clustering Molecular Dynamics Trajectories: 1. Characterizing the Performance of Different Clustering Algorithms. *J. Chem. Theory Comput.* **2007**, *3*, 2312–2334.
58. Lavery, R.; Moakher, M.; Maddocks, J. H.; Petkeviciute, D.; Zakrzewska, K. Conformational Analysis of Nucleic Acids Revisited: Curves+. *Nucleic Acids Res.* **2009**, *37*, 5917–5929.
59. Tomasi, J.; Mennucci, B.; Cammi, R. Quantum Mechanical Continuum Solvation Models. *Chem. Rev.* **2005**, *105*, 2999–3093.
60. Dederichs, P. H.; Blugel, S.; Zeller, R.; Akai, H. Ground States of Constrained Systems: Application to Cerium Impurities. *Phys. Rev. Lett.* **1984**, *53*, 2512–2515.
61. Wesolowski, T. A.; Warshel, A. Frozen Density-Functional Approach for *Ab Initio* Calculations of Solvated Molecules. *J. Phys. Chem.* **1993**, *97*, 8050–8053.
62. Wu, Q.; Van Voorhis, T. Direct Optimization Method to Study Constrained Systems within Density-Functional Theory. *Phys. Rev. A* **2005**, *72*, 024502.
63. Jorgensen, W. L.; Chandrasekhar, J.; Madura, J. D.; Impey, R. W.; Klein, M. L. Comparison of Simple Potential Functions for Simulating Liquid Water. *J. Chem. Phys.* **1983**, *79*, 926–935.
64. Cubero, E.; Guimil-Garcia, R.; Luque, F. J.; Eritja, R.; Orozco, M. The Effect of Amino Groups on the Stability of DNA Duplexes and Triplexes Based on Purines Derived from Inosine. *Nucleic Acids Res.* **2001**, *29*, 2522–2534.
65. Migliore, A. Full-Electron Calculation of Effective Electronic Couplings and Excitation Energies of Charge Transfer States: Application to Hole Transfer in DNA π-stacks. *J. Chem. Phys.* **2009**, *131*, 114113.
66. Migliore, A.; Corni, S.; Di Felice, R.; Molinari, E. First-Principles Density-Functional Theory Calculations of Electron-Transfer Rates in Azurin Dimers. *J. Chem. Phys.* **2006**, *124*, 064501.
67. Becke, A. D. Density-Functional Thermochemistry .3. The Role of Exact Exchange. *J. Chem. Phys.* **1993**, *98*, 5648–5652.
68. Wong, B. M.; Piacenza, M.; Della Sala, F. Absorption and Fluorescence Properties of Oligothiophene Biomarkers from Long-Range-Corrected Time-Dependent Density Functional Theory. *Phys. Chem. Chem. Phys.* **2009**, *11*, 4498–4508.
69. Senthilkumar, K.; Grozema, F. C.; Bickelhaupt, F. M.; Siebbeles, L. D. A. Charge Transport in Columnar Stacked Triphenylenes: Effects of Conformational Fluctuations on Charge Transfer Integrals and Site Energies. *J. Chem. Phys.* **2003**, *119*, 9809–9817.